Asian Journal of Chemistry; Vol. 33, No. 8 (2021), 1891-1904

ASIAN JOURNAL OF CHEMISTRY

https://doi.org/10.14233/ajchem.2021.23304

Structural and Vibrational Spectroscopic Elucidation of Nitrogen Rich Energetic Salt: 2,4-Diamino-6-methyl-1,3,5-triazinium Levulinate Dihydrate

K. Ayisha Begam[1], N. Kanagathara[2,*], V. Ragavendran[3], R. Gowri Shankar Rao[4] and M.K. Marchewka[5]

[1]Department of Physics, Saveetha Engineering College, Thandalam, Chennai-602105, India
[2]Department of Physics, Saveetha School of Engineering, Saveetha Institute of Medical and Technical Sciences, Thandalam, Chennai-602105, India
[3]Department of Physics, Sri Chandrasekharendra Saraswathi Viswa Mahavidyalaya, Enathur, Kanchipuram-631561, India
[4]Department of Physics, Vel Tech Rangarajan Dr.Sagunthala R&D Institute of Science and Technology, Chennai-600062, India
[5]Institute of Low Temperature and Structure Research, Polish Academy of Sciences, 50-950 Wroclaw, 2, P.O. Box 937, Poland

*Corresponding author: E-mail: kanagathara23275@gmail.com

Received: 14 May 2021; *Accepted*: 14 June 2021; *Published online*: 26 July 2021; AJC-20443

A novel nitrogen rich energetic salt 2,4-diamino-6-methyl-1,3,5-triazinium levulinate dihydrate (DMTLDH) has been grown by slow evaporation method at room temperature. The grown synthesized salt crystallizes in the centrosymmetric space group $P2_1/n$ of monoclinic system. The intermolecular hydrogen bond N–H···N, N–H···O, C–H···O, O–H···O type interactions stabilizes the structure and leads to three dimensional network. In addition to that the crystal structure also possesses C–O···Cg interactions. Also, quantum chemical computational studies using DFT-B3LYP/6-311++G(d,p) and PBEPBE/6-31G(d,p) basis set is used to analyze the structural parameters and vibrational frequencies of grown crystal. Frontier molecular orbital analysis describes the charge transfer within the molecule and also other electronics parameters were calculated. The natural bonding orbital analysis has also been performed to study the stability of the molecule. Further, the crystal packing behaviour of DMTLDH was studied quantitatively with the aid of Hirshfeld surface analysis.

Keywords: Crystal structure, Hydrogen bond, XRD, DFT, NBO, Hirshfeld surface analysis.

INTRODUCTION

s-Triazine derivatives are perceived to be a significant class of materials in the field of biology, medicinal chemistry, pharmaceutical industry and polymer chemistry. It is well known that these derivatives can be used as a liquid crystals, metal complexes and new hydrogenation catalysts [1]. Due to its nitrogen-rich structure, *s*-triazine attracts the interest of researchers in the field of energetic materials and explosives [2]. Nitrogen based energetic materials includes explosives, pyrotechnics and propellants, are widely used for military and civilian applications due to its high thermal stability and density because of the existence of C–N and N-N bonds. The low vapour pressure and high density makes the salt based energetic materials to be better than non-ionic molecule. 1,3,5-Triazine derivatives are widely used as a fire retarding additives in resin and susceptible to nucleophilic attack [3]. It is also found that these *s*-triazine derivatives form self-assembling nanostructures on metallic surfaces. Benassi *et al.* [4] reported the theoretical analysis of structural as well as vibrational properties of *s*-triazine derivatives. Earlier researchers [5,6] investigated the *s*-triazine complexes and its derivatives of metal ions theoretically. The N–H···N, N–H···O and O–H···O interactions gives rise to 3D supramolecular structure of their compound and ensure the presence of intermolecular interactions between the compounds. In continuation of interest in the study of *s*-triazine compounds, 6-methyl-1,3,5-triazine-2,4-diamine (DMT) is taken as the subject of examination. Sangeetha *et al.* [7] reported the asymmetric unit of DMT with trichloroacetic acid. Xiao *et al.* [8] synthesized organic-inorganic high dimensional supramolecular structure of DMT by using hydroxyl benzoic acid and nitric acid as a structural building block. The crystalline complex of 3,5-dihydroxybenzoic acid with DMT is an excellent supramolecular structure in which 3,5-dihydroxy-benzoic acid has robust hydrogen-bonding donors/acceptors to satisfy the diversiform motifs. DMT dinitramide complex was reported by Xiao

This is an open access journal, and articles are distributed under the terms of the Attribution 4.0 International (CC BY 4.0) License. This license lets others distribute, remix, tweak, and build upon your work, even commercially, as long as they credit the author for the original creation. You must give appropriate credit, provide a link to the license, and indicate if changes were made.

et al. [9]. Thermal decomposition kinetics analysis have also been carried out and found that the thermal decomposition resistance exist up to 470 K in silver dinitramide and DMT perchlorate compounds. DMT with various salts of silver was investigated by Chen *et al.* [10]. Their findings shows that 1D polymer with metallamacrocycles based silver salt building unit form a 3D open network by hydrogen. The existence of hydrogen bond donor and acceptor in the carboxylic group makes its importance in crystal engineering. Compounds of N-heterocyclic group are identified as building blocks for the arrangement of supramolecular structure of compounds under different hydrogen bond associations. Mary [11] reported the vibrational spectroscopic and computational study of DMT 4-cyanobenzoate. Perpetuo & Janczak [12] and Narimani & Yamin [13] investigated the structure of DMT with trifluoroacetic acid and oxalic acid, respectively. Begam *et al.* [14] reported the theoretical investigation of structural, vibrational as well as other electronic properties of DMT with trifluroacetic acid.

Levulinic acid is an industrial chemical used as a starting material for pharmaceuticals, plasticizers, resin, textile and additives. It is a biodegradable herbicide and used in cosmetics. The therapeutic utilization of metal organic salts relies upon the organic part of the molecule to where the metal ion is appended. This part influences the solubility of salt, pH and stability. Derived heterocyclic compounds of levulinic acid are employed as bacteriostatic and analgesic agents [15]. Continuation in research on hydrogen bond formation in *s*-triazine derivatives in solid state is yet proceeding because of its ability to develop well define supramolecular engineering. In the present work, it is aimed to synthesize the complex of DMT with levulinic acid in order to analyze the physico chemical properties of the obtained salt that form multiple N–H···N, N–H···O hydrogen bond sites. To the extent all the authors' knowledge concerned, the structure as well as all other properties of the DMT with levulinic acid is reported first time. Theoretical calculations are carried out with B3LYP hybrid functional using 6-311++G(d,p) and PBEPBE/6-31G(d,p) basis set. The NBO, HOMO-LUMO, hyper-polarizability calculations and Hirshfeld surface analysis has been done to get complete knowledge about the grown compound.

EXPERIMENTAL

Synthesis: Analytical grade of 2,4-diamino-6-methyl-1,3,5-triazine (**1**) and levulinic acid (**2**) were taken as the starting materials for synthesizing 2,4-diamino-6-methyl-1,3,5-triazinium levulinate dihydrate (DMTLDH) (**3**). A solution was prepared by dissolving 2,4-diamino-6-methyl-1,3,5-triazine and levulinic acid in water with 1:1 molar ratio and stirred well to get homogeneous solution. The solution was then allowed to evaporate at room temperature. Subsequently, the solution reached super saturation state and lead to nucleation followed by the growth mechanism. Well-developed colourless crystals of DMTLDH were harvested after a period of 20 days. Further purification is done by recrystallization process (**Scheme-I**). Fig. 1 shows the photograph of as developed crystal.

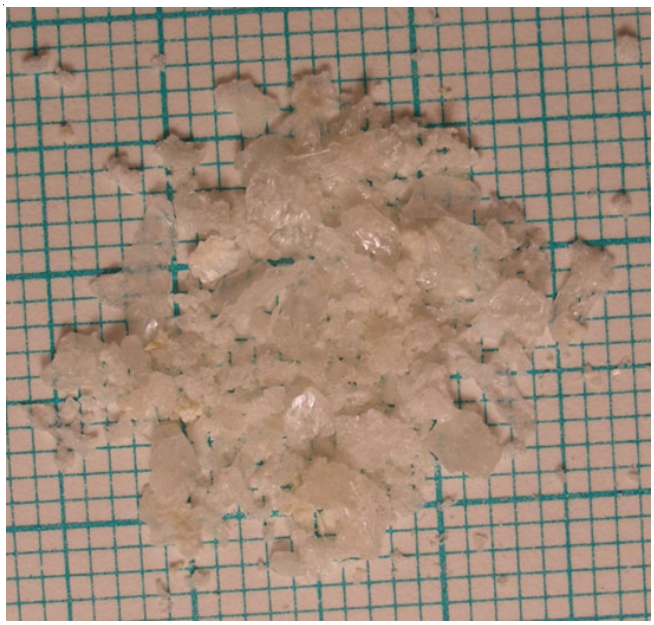

Fig. 1. Photograph of as-grown DMTLDH

Quantum chemical computations: Gaussian 09 program with B3LYP/6-311++G(d,p) and PBEPBE/6-31G(d,p) basis set is employed to perform quantum chemical calculations to understand the structure and vibrational wavenumbers of the synthesized crystal [16]. Single crystal XRD output is used as input to run the theoretical calculations. Scaling procedures in DFT computations are helpful to improve the wavenumbers on vibrational spectra. Generally scaling factor value of 0.9665 is used for the B3LYP/6-311++G(d,p) basis set and 0.986 is used for the PBEPBE/6-31g(d,p) basis set to correct the calculated harmonic frequencies, infrared and Raman intensities [16]. The absence of negative frequencies on the computed vibrational data confirms the optimized structure with global minimum. The NBO computations are executed with the aid of NBO 5.1 program as built in the Gaussian 09W package to elucidate the various second order interactions between the filled and vacant orbital of one subsystem to another subsystem [17]. The time dependent-density functional theory (TD-DFT) method is applied to get UV-visible spectrum. The graphic illustrations

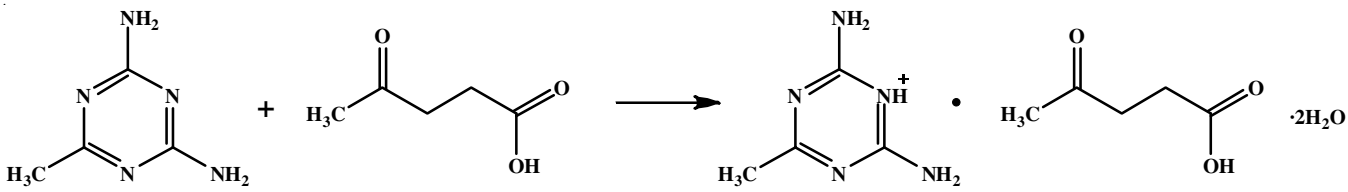

Scheme-I

with isosurface value 0.001 was used in the case of HOMO-LUMO analysis [18]. MERCURY 3.8 [19] software was used to simulate powder X-ray diffraction pattern of the developed crystal by giving crystallographic information file as the input. The simulated powder X-ray diffraction pattern was generated from the crystallographic informaion file obtained from single crystal XRD data using the freely available CCDC Mercury software.

Spectroscopic measurements: Infrared spectra were recorded with a Bruker IFS-88 spectrometer in the region 4000-400 cm^{-1} while powder Fourier transform Raman (FT-Raman) spectra were recorded with an FRA-106 attachment to the Bruker IFS-88 spectrometer equipped with Ge detector cooled to liquid nitrogen temperature. Resolution was set up to 2 cm^{-1}, signal/noise ratio was established by 32 scans, weak apodization. Nd^{3+}: YAG air-cooled diode pumped laser of power of 200 mW was used as an exciting source. The incident laser excitation is 1064 nm. The scattered light was collected at the angle of 180º in the region 3600-80 cm^{-1}. Due to the poor detector response, the Raman counterparts of the infrared bands located above 3200 cm^{-1} were not observed in the spectrum.

Molecular Hirshfeld surface calculations: The size and shape of Hirshfeld surface lend visualization of intermolecular close contact in molecular crystals [20]. 3D Hirshfeld surfaces and 2D finger plots of the title compound is obtained by giving cif as the input using Crystal Explorer 3.1 software [21]. Hirshfeld surfaces are constructed based on electron distribution which is calculated as sum of spherical atom electron densities [22]. The normalized contact distance d_{norm} depend on the distance from a point on the surface to the nearest nucleus outside the surface, d_e is the distance from a point on the surface to the nearest nucleus inside the surface, d_i enables the identification of the regions of particular importance to the intermolecular interactions. The intermolecular contacts in the crystal lattice is contributed by the combination of d_e and d_i in the form of two-dimensional fingerprint plot [23]. It helps to generate Hirshfeld surfaces that mapped with d_{norm}, shape index, curvedness and 2D fingerprints. The normalized contact distance $d_{norm} = d_i - r_i^{vdw}/r_i^{vdw} + d_e - r_e^{vdw}/r_e^{vdw}$ where r_i^{vdw} and r_e^{vdw} are the van der Waals radii of the atoms.The intermolecular contact is shorter than r^{vdw} if d_{norm} is negative and longer if d_{norm} is positive. The red-white-blue colour in Hirshfeld surface map exemplifies the shortest intermolecular contact, contact around r^{vdw} separation and longer intermolecular contact distance, respectively. The 2D fingerplot is a combination of d_e and d_i provides the summary of intermolecular contacts in the crystal and are in complement to the Hirshfeld surfaces [24]. Based on the local curvature of the surface the coloured properties like shape index and curvedness can also be specified.

RESULTS AND DISCUSSION

Single crystal X-ray diffraction analysis: X-ray diffraction intensity data were collected on four circle KUMA KM-4 single crystal X-ray diffractometer furnished with graphite monochromated Mo*K*α (λ = 0.7103 Å) radiation and CCD detector. Crystals of measurement 0.40 mm × 0.38 mm × 0.10 mm were sliced to appropriate size and mounted on a glass fibre using cyanoacrylate adhesive. The unit cell parameters were resolved from 36 frames measured (0.5º phi-scan) from three different crystallographic zones and utilizing the strategy of difference vectors. The intensity data were collected with an average four-fold redundancy per reflection and optimum resolution (0.75 Å). The intensity data collection, frames integration, Lorentz and polarization correction as well as decay correction were done using KUMA KM-4 CCD software [25]. Empirical absorption correction (multi-scan) was performed using SHELXTL program [26]. SHELXL-97 program direct method is chosen for structure solution and refinement [27]. The compound crystallizes in monoclinic $P2_1/n$ space group with four molecules in the asymmetric unit. Initially, the structure was refined with isotropic thermal parameters. In final refinement all non-hydrogen atoms were refined with anisotropic thermal parameters by full-matrix least-squares methods by means of SHELXL97 program. Scattering factors for neutral atoms and calculations for anomalous dispersion were as in SHELXL97 program [27].

Single crystal X-ray diffraction data confirms that the grown crystal crystallizes in monoclinic crystal system with centrosymmetric space group $P2_1/n$. The lattice parameters are determined to be a = 7.6580(11) Å, b = 17.598(2) Å, c = 10.8428(16) Å, α = β = 90º, γ = 110.289(13)º. The volume of the unit cell is determined to be = 1370.6(3) $(Å)^3$. Details of the data collection parameters, crystallographic data and final agreement factors are collected in Table-1. Chosen bond distances and angles results from single crystal XRD data along with theoretically obtained results from both B3LYP/6-311++G(d,p) and

TABLE-1
CRYSTAL DATA AND STRUCTURE REFINEMENT OF DMTLDH

Empirical formula	$C_9H_{19}N_5O_5$
Formula weight (g mol^{-1})	277.29
Temperature (K)	295(2)
Wavelength (A)	0.71073 Å
Crystal system	Monoclinic
Space group	P 2(1)/n
a	7.6580(11) Å
b	17.598(2) Å
c	10.8428(16) Å
α	90°
β	110.289(13)°
γ	90°
V	1370.6(3) $(Å)^3$
Z	4
D_{calc} (Mg m^{-3})	1.344
Absorption coefficient (mm^{-1})	0.110
F(000)	592
Crystal size (mm)	0.40 × 0.38 × 0.10
Theta range for data collection (°)	2.85-27.48
Index ranges	h = -9 → 9; k= -22 → 22; l = -14 → 14
Completeness to θ	100%
Refinement method	Full-matrix least squares on F^2
Data/restraints/parameters	3121/0/177
Goodness of fit on F^2	0.937
Largest differences peak and hole (e. $Å^{-3}$)	0.321 and –0.249

PBEPBE/6-31G(d,p) are recorded in Table-2. The asymmetric unit of DMTLDH is shaped by the one protonated DMT cation and one deprotonated levulinate anion with two water molecules. All the bond angles and bond distances are within the expected range. The obtained parameters are well in concurrence with theoretical values. Atomic displacement parameters tabulated in Table-3. Fractional atomic coordinates and isotropic or equivalent isotropic displacement parameters are listed in Table-4. The non hydrogen triazine ring, C1/N1/C2/N2/C3/N3, is planar with a maximum deviation of 0.035 (1) Å from the least square plane for N3 atom. The levulinate anion O1/C1/O2/C2/O3/O4, is less planar with a maximum deviation of 0.131 (1) Å for O1 and O4 atoms. The bond lengths and angles are in normal ranges [17,18]. It is seen from the Table-2 that B3LYP/6-311+G(d,p) basis set results are almost similar with experimental data. Fig. 2 represents the ORTEP plot of DMTLDH with the atom numbering scheme. Fig. 3 drawn the packing diagram of DMTLDH. In the crystal structure the molecules are connected by N–H···O, N–H···N, O–H···O and C–H···O intermolecular hydrogen bonds (symmetry codes as in Table-2) to form a three-dimensional network (Fig. 4). In addition, there are weak π–π interactions between the triazine ring centroids Cg1 (symmetry code: 1-x, -y, 1-z) with a distance of 3.763 Å and a C6–O3···π involving the triazine (C1/N1/C2/N2/C3/N3) centroid (symmetry code: 1-x, 1-y, 1z) with a O3···Cg1 distance of 3.5300 (16) Å and a C6–O3–Cg1 bond angle of 132.19 (10)º. Kavitha *et al.* [7]

TABLE-2
SELECTED BOND DISTANCES (Å) AND BOND ANGLES (°) DMTLDH

Atom	Expt.	PBEPBE 6-31G(d,p)	B3LYP 6-311++G(d,p)	Atom	Expt.	PBEPBE 6-31G(d,p)	B3LYP 6-311++G(d,p)
Bond distance (Å)							
N1A-C6A	1.343	1.325	1.312	C1B-O11B	1.241	1.288	1.273
N1A-C2A	1.355	1.374	1.364	C1B-C2B	1.507	1.532	1.526
N1A-H1N1	0.990	1.109	1.079	C2B-C3B	1.515	1.525	1.524
C2A-N2A	1.313	1.351	1.343	C2B-H1C2	0.970	1.102	1.093
C2A-N3A	1.332	1.345	1.332	C2B-H2C2	0.970	1.104	1.093
N2A-H1N2	0.860	1.013	1.006	C3B-H1C3	0.970	1.105	1.094
N2A-H2N2	0.866	1.014	1.006	C3B-H2C3	0.970	1.107	1.098
N3A-C4A	1.339	1.346	1.336	C4B-O41B	1.210	1.231	1.214
C4A- N4A	1.317	1.329	1.321	C4B-C5B	1.482	1.518	1.513
C4A-N5A	1.369	1.383	1.374	C5B-H1C5	0.960	1.106	1.095
N4A-H1N4	0.860	1.016	1.008	C5B-H2C5	0.960	1.100	1.089
N4A-H2N4	0.860	1.054	1.039	C5B-H3C5	0.960	1.101	1.093
N5A-C6A	1.306	1.363	1.357	O1W-H1W1	0.830	0.993	0.978
C6A-C7A	1.475	1.494	1.491	O1W-H2W1	0.830	0.973	0.961
C7A-H1C7	0.960	1.103	1.093	O2W-H1W2	0.885	0.983	0.962
C7 A-H2C7	0.960	1.112	1.095	O2W-H2W2	0.840	0.976	0.972
C7A-H3C7	0.960	1.097	1.087	C3B-C4B	1.486	1.525	1.522
Bond angle (°)							
H1C7-C7A-H3C7	109.5	110.46	110.29	C6A-N1A-C2A	119.32	114.67	115.59
H2C7-C7A-H3C7	109.5	106.98	106.62	C6A-N1A-H1N1	118.7	114.67	117.66
O11B-C1B-O12B	122.93	124.18	123.84	C2A-N1A-H1N1	121.10	122.50	120.39
O11B-C1B-C2B	120.34	115.98	116.36	N2A-C2A-N3A	120.53	117.34	117.83
O12B-C1B-C2B	116.71	119.81	119.78	N2A-C2A-N1A	117.96	115.17	115.72
C1B-C2B-C3B	114.78	113.67	114.80	N3A-C2A-N1A	121.50	127.47	126.44
C1B-C2B-H1C2	108.6	107.05	107.19	C2A-N2A-H1N2	120.0	118.93	119.30
C3B-C2B-H1C2	108.6	110.90	110.18	C2A-N2A-H2N2	120	119.52	119.76
C1B-C2B-H2C2	108.6	107.76	107.20	H1N2-N2A-H2N2	120.	121.30	120.92
C3B-C2B-H2C2	108.6	110.50	110.62	C2A-N3A-C4A	115.72	114.75	115.74
HIC2-C2B-H2C2	107.5	106.60	106.43	N4A-C4A-N3A	119.18	121.53	121.20
N3A-C4A-N5A	125.27	121.56	120.91	N4A-C4A-N5A	115.55	116.90	117.87
C4A-N4A-H1N4	120	119.48	118.52	N5A-C6A-C7A	119.88	117.23	117.66
C4A-N4A-H2N4	120	120.86	121.58	N1A-C6A-C7A	117.66	120.25	120.39
H1N4-N4A-H2N4	120	118.20	119.88	C6A-C7A-H1C7	109.5	110.79	111.04
C6A-N5A-C4A	115.67	119.00	119.33	C6A-C7A-H2C7	109.5	109.25	109.26
N5A-C6A-N1A	122.45	122.50	121.93	H1C7-C7A-H2C7	109.5	110.46	110.29
C4B-C3B-C2B	115.54	113.36	114.62	C6A-C7A-H3C7	109.5	109.94	109.93
C4B-C3B-H1C3	108.4	107.57	106.17	O41B-C4B-C3B	121.51	121.72	122.11
C2B-C3B-H1C3	108.4	111.14	109.99	C5B-C4B-C3B	116.6	117.13	116.25
C4B-C3B-H2C3	108.4	107.72	108.52	C4B-C5B-H1C5	109.5	105.97	108.08
C2B-C3B-H2C3	108.4	110.89	111.15	C4B-C5B-H2C5	109.5	110.04	110.17
HIC3-C3B-H2C3	107.5	105.76	105.88	H1C5-C5B-H2C5	109.5	107.38	108.56
O41B-C4B-C5B	121.9	121.07	121.63	C4B-C5B-H3C5	109.5	113.50	111.81
H1C5-C5B-H3C5	109.5	107.38	108.56	H1W1-O1W-H2W1	107.0	102.56	105.74
H2C5-C5B-H3C5	109.5	110.53	110.42	H1W2-O2W-H2W2	94.6	100.48	104.00

TABLE-3
ATOMIC DISPLACEMENT PARAMETERS (Å^2)

Atom	U11	U22	U33	U23	U13	U12
N1A	0.0360(9)	0.0398(9)	0.0305(9)	0.0052(7)	0.116(7)	0.0075(7)
C2A	0.0370(11)	0.0361(10)	0.0312(10)	0.0044(8)	0.0123(9)	0.0031(9)
N2A	0.0483(11)	0.0663(12)	0.0298(9)	0.0094(8)	0.0152(8)	0.0200(9)
N3A	0.0396(10)	0.0485(10)	0.0292(9)	0.0052(7)	0.0139(7)	0.0072(8)
C4A	0.00356(11)	0.0373(11)	0.0326(11)	0.0019(8)	0.0115(9)	0.0006(8)
N4A	0.0388(10)	0.0701(12)	0.0312(9)	0.0059(8)	0.0124(8)	0.0140(8)
N5A	0.0385(10)	0.0453(9)	0.0303(8)	0.0025(7)	0.0125(7)	0.0074(7)
C6A	0.0396(12)	0.0342(11)	0.0348(11)	0.0010(8)	0.0151(9)	0.0015(8)
C7A	0.0489(13)	0.0670(15)	0.0422(12)	0.0031(10)	0.0199(10)	0.0151(11)
C1B	0.0375(11)	0.0397(11)	0.0409(12)	0.0064(9)	0.0154(9)	0.0020(9)
O11B	0.0510(9)	0.0520(9)	0.0432(8)	0.0032(6)	0.0194(7)	0.0123(7)
O12B	0.0523(9)	0.0756(11)	0.0377(9)	0.0074(7)	0.0159(7)	0.0230(8)
C2B	0.0404(12)	0.0630(15)	0.0487(13)	0.014(11)	0.0158(10)	0.0111(10)
C3B	0.0381(12)	0.0678(16)	0.0470(13)	0.0137(11)	0.0061(10)	0.0057(10)
C4B	0.0369(12)	0.0468(13)	0.0416(12)	0.0074(10)	0.0066(10)	0.0114(10)
O41B	0.0563(10)	0.0566(10)	0.0585(10)	0.0014(8)	0.0163(8)	-0.0031(8)
C5B	0.0690(17)	0.0913(19)	0.0453(14)	0.0080(120	0.0179(12)	0.0044(14)
O1W	0.0939(13)	0.0857(12)	0.0946(13)	0.0269(10)	0.0636(11)	0.0395(10)
O2W	0.0719(12)	0.0999(14)	0.1073(15)	0.0281(11)	0.0496(11)	0.0014(10)

TABLE-4
FRACTIONAL ATOMIC COORDINATES AND ISOTROPIC OR EQUIVALENT ISOTROPIC DISPLACEMENT PARAMETERS (Å^2)

Atom	x	y	Z	U iso or equi
N1A-N	0.6595(2)	0.06909(9)	0.62717(15)	0.0354(4)
H1N1-H	0.548(3)	0.0962(10)	0.5688(18)	0.042
C2A-C	0.7950(3)	0.04516(9)	0.58254(18)	0.0348(4)
N2A-N	0.7628(2)	0.04916(9)	0.45562(14)	0.0477(5)
H1N2-H	0.8455	0.0337	0.4243	0.057
H2N2-H	0.6590	0.0673	0.4038	0.057
N3A-N	0.9552(2)	0.01720(9)	0.66377(14)	0.0386(4)
C4A-C	0.9752(3)	0.09615(10)	0.79146(18)	0.0353(4)
N4A-N	1.1301(2)	-0.00984(9)	0.87775(15)	0.0467(5)
H1N4-H	1.2169	-0.0269	0.8518	0.056
H2N4-H	1.1446	-0.0103	0.9600	0.056
N5A-N	0.8457(2)	0.04262(9)	0.84248(14)	0.0378(4)
C6A-C	0.6897(3)	0.06708(10)	0.75677(18)	0.0356(4)
C7A-C	0.5378(3)	0.09258(13)	0.8012(2)	0.0516(6)
H1C7-H	0.4662	0.0494	0.8098	0.077
H2C7-H	0.4589	0.1273	0.7380	0.077
H3C7-H	0.5895	0.1176	0.8847	0.077
C1B-C	0.3141(3)	0/14010(11)	0/35537(19)	0.0389(5)
O11B-O	0.40601(18)	0.10454(7)	0.29995(13)	0.0479(4)
O12B-O	0.35646(19)	0.14162(8)	0.47908(13)	0.0552(4)
C2B-C	0.1413(3)	0.18275(12)	0.27548(19)	0.0506(6)
H1C2-H	0.1533	0.2351	0.3053	0.061
H2C2-H	0.0355	0.1609	0.2925	0.061
C3B-C	0.1009(3)	0.18212(13)	0.12850(19)	0.0532(6)
H1C3-H	0.1110	0.1302	0.1015	0.064
H2C3-H	-0.0268	0.1982	0.0847	0.064
C4B-C	0.2239(3)	0.23088(12)	0.0820(2)	0.0436(5)
O41B-O	0.3309(2)	0.27572(8)	0.15437(15)	0.0581(4)
C5B-C	0.2088(3)	0.22167(14)	-0.0572(2)	0.0691(7)
H1C5-H	0.2775	0.2614	-0.0806	0.104
H2C5-H	0.0803	0.2245	-0.1127	0.104
H3C5-H	0.2588	0.1732	-0.0685	0.104
O1W-O	0.6172(2)	0.11840(10)	0.14422(17)	0.0833(6)
H1W1-H	0.6393	0.1638	0.1349	0.125
H2W1-H	0.5465	0.1173	0.1876	0.125
O2W-O	0.6847(2)	0.27354(11)	0.11702(19)	0.0881(6)
H1W2-H	0.7147	0.3071	0.0668	0.132
H2W2-H	0.5930	0.2985	0.1207	0.132

TABLE-5
HYDROGEN BOND GEOMETRY (Å, °)

D-H···A	D···H	H···A	D···A	D-H···A
N1A-H1N1···O12B	0.990(19)	1.66(2)	2.647(2)	176.2(17)
N2A-H1N2···N3A	0.86(2)	2.25	3.105(2)	174.4
N2A-H2N2···O11B	0.86	1.98	2.804(2)	173.0
N4A-H2N4···N5A	0.86	2.19	3.030(2)	164.7
N4A-H1N4···O1W	0.86	2.04	2.787(2)	144.4
O1W-H1W1···O2W	0.83	1.98	2.813(3)	177.4
O1W-H2W1···O11B	0.83	1.90	2.724(2)	172.5
O2W-H1W2···O12B	0.89	1.90	2.750(2)	159.9
O2W-H2W2···O41B	0.84	2.20	2.875(2)	137.6

Symmetry codes: (i) x, y, z ; (ii) -x+1/2, y+1/2, -z+1/2; (iii) –x, -y, -z ; (iv) x-1/2, -y-1/2, z-1/2

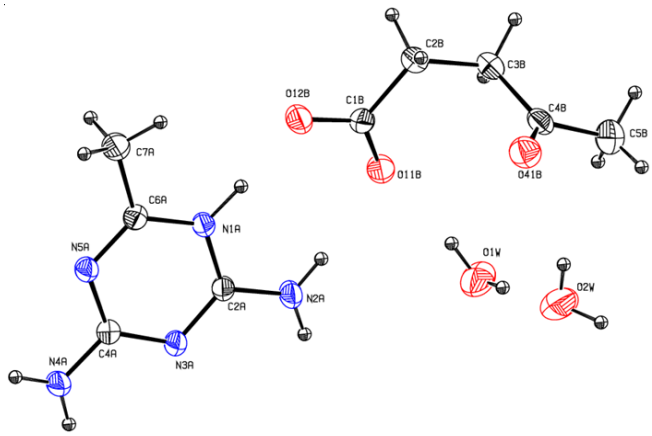

Fig. 2. The ORTEP plot of DMTLDH with the atom numbering Scheme. Displacement ellipsoids are drawn at 30% probability level

reported the interaction between the amino group and aromatic ring establishes a small displacement of the nitrogen atom out of the benzene ring with a torsional angle of N11-C1-C2-C3 in 177°. The triazine ring (N1A/C2A/N3A/C4A/N5A/C6A) makes a dihedral angle of 21.6 (2)° with the levulinic acid (C1B-C5B) molecule. The triazine ring embraces a planar

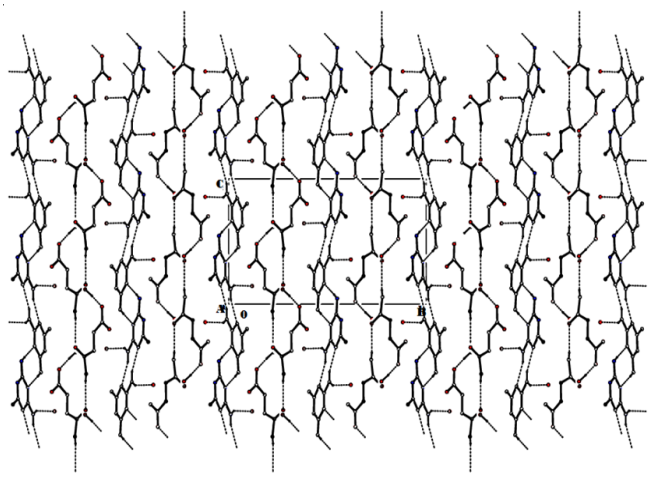

Fig. 3. Molecular packing of DMTLDH forming a 3-dimensional network

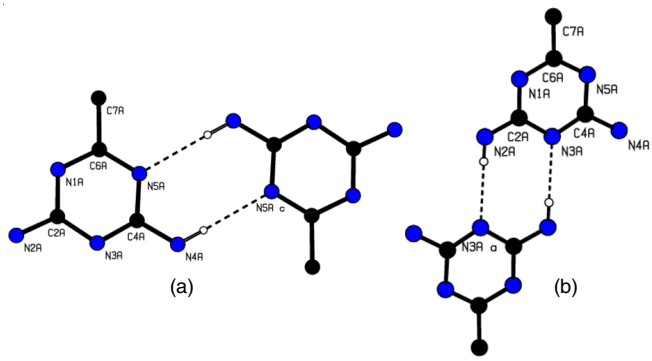

Fig. 4. The compound DMTLDH forming R_2^2 (8) ring motif due to N–H···N hydrogen bonds

conformation with N1A and N3A atoms having a minimum deviation of -0.008(2) Å. The crystal structure forms N4A–H2N4···N5A, N2A–H1N2···N3A interactions which forms R_2^2 (8) ring motifs (Fig. 4). Further the crystal structure is stabilized intermolecular N–H···N, N–H···O, C–H···O, O–H···O hydrogen bonds which leads to a formation of a three dimensional network. Besides these interactions, the structure also possesses C–O···Cg interactions (Fig. 5 and Table-6). Fig. 6 depicts the optimized structure of DMTLDH obtained by DFT/B3LYP-6-311++G(d,p) basis set.

TABLE-6
C–O···Cg FOR COMPOUND 295 (Å)

D–H···A	D···A
C1B–O11B···Cg1^{i}	3.1008(2)
C1B–O12B···Cg1^{i}	3.8328(2)
C1B–O12B···Cg1^{ii}	3.2542(2)

Cg1 is the centroid of the ring (N1A/C2A/N3A/C4A/N5A/C6A)
Symmetry codes: (i) 1-x,-y, 1-z ii) -1/2+x, 1/2-y,-1/2+z

Powder XRD studies: Powder X-ray diffraction studies was performed theoretically to recognize the crystalline nature of the developed crystal. The outcome of the powder X-ray diffraction are calculated with the aid of Mercury 3.8 software. Fig. 7 depicts the simulated powder X-ray diffraction pattern of the grown crystal. The crystallite size (D) was calculated by Debye-Scherrer's formula using equation:

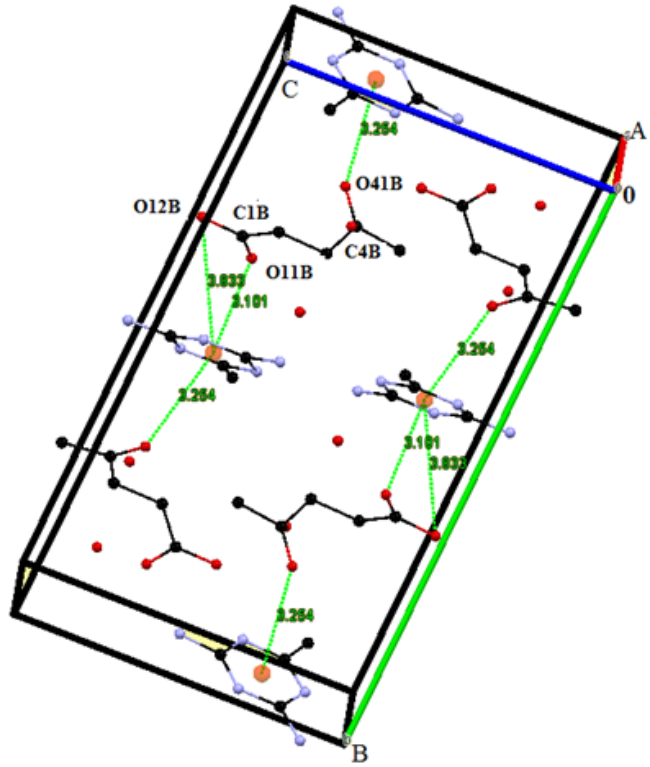

Fig. 5. Molecular packing of DMTLDH forming a C–O···Cg interactions

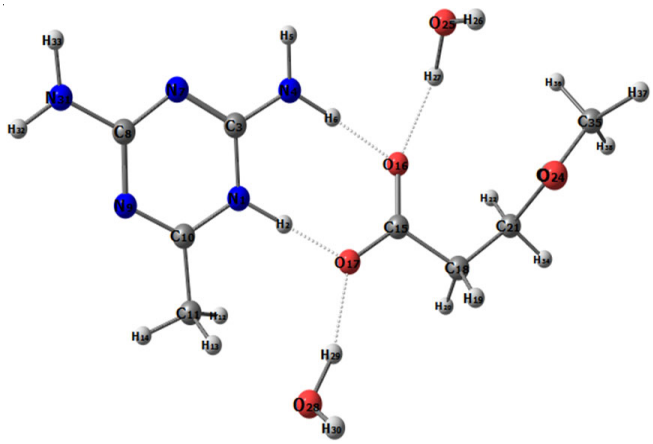

Fig. 6. Optimized structure of DMTLDH

$$D = \frac{K\lambda}{\beta_{1/2}\cos\theta}$$

As the powder sample was taken for XRD, the impact of the strain, instruments and other obscure factor causing the broadening of the peak were disregarded. The mean value of the crystallite size of DMTLDH is discovered to be 14.203 μm.

Vibrational bands assignment description: The FT-IR and FT Raman spectrum of 2,4-diamino-6-methyl-1,3,5-triazin-1-ium levulinate dihydrate (DMTLDH) was recorded and investigated. The vibrational wavenumbers were computed using B3LYP/6-311++G(d,p) and PBEPBE/6-31G(d,p) basis set. The data got from vibrational wavenumber calculations with potential energy distribution analysis are utilized to assign

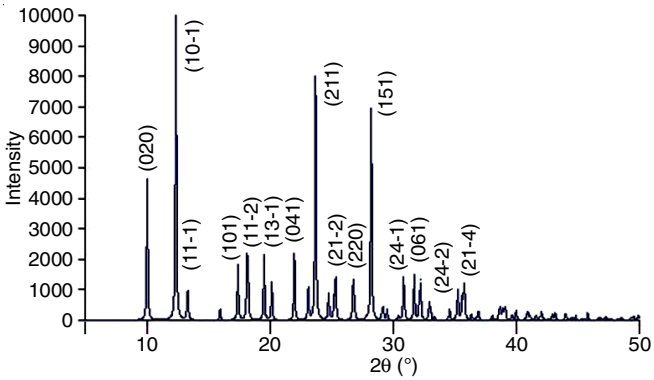

Fig. 7. Simulated powder X-ray diffraction pattern of DMTLDH

vibrational bands acquired in infrared and FT Raman spectroscopy of the studied molecule. Intense hydrogen-bonded network is present in the crystal structure of the complex with noticeable vibrational effects. Table-7 gives the theoretical and experimental values for the computed frequencies. Figs. 8 and 9 gives the experimental FT-IR and FT Raman spectrum of DMTLDH. Theoretically predicted FT-IR and FT Raman spectrum by B3LYP/6-311++G(d,p) and PBEPBE/6-31G(d,p) basis set is shown in Figs. 10 and 11, respectively. The internal vibrations of the DMT cations and levulinate anions contribute its signature in the region between 4000-400 cm^{-1}. The lattice vibrations are observed in the Raman spectrum bands below 200 cm^{-1}.

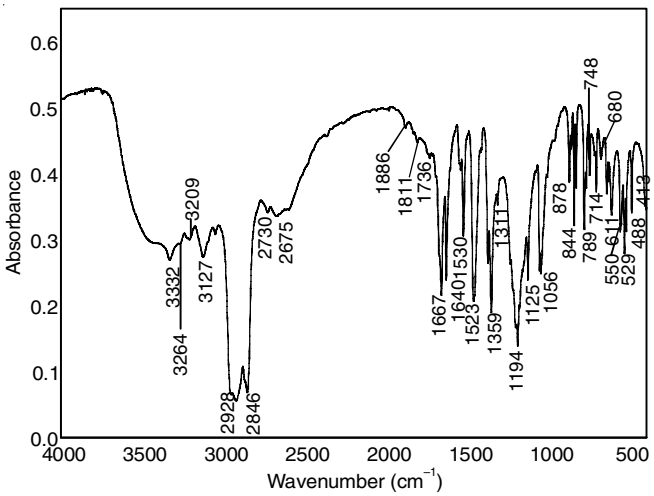

Fig. 8. FT-IR spectrum of DMTLDH

Vibrational bands of 2,4-diamino-6-methyl-1,3,5-triazinium (DMT) cation: DMT residues form hydrogen bonds of N–H···O and N–H···N types of interaction with distance of 2.647 Å 3.105 Å, respectively. DMT cations exhibit C–N, C–C, C–H and N–H vibrations. The symmetric stretching oscillations of the NH_2 groups are in general electron donating group and lie in the range of 3450-3250 cm^{-1} [28]. N–H stretching vibrational frequency occurs at 3328 cm^{-1} in 1,3,5-triazine derivatives by Fernandez-Liencres *et al.* [29]. In present work, compound DMTLDH, asymmetric and symmetric stretching vibrations of N–H occur at 3264, 3209, 3127, 2928, 2846, 2730, 2675 cm^{-1} in infrared spectrum. This peak is observed at 2968 cm^{-1} in FT Raman spectrum. Theoretically predicted amino group

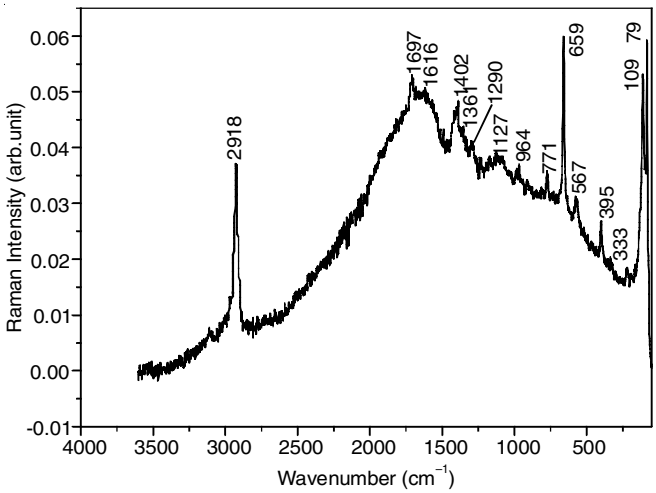

Fig. 9. FT Raman spectrum of DMTLDH

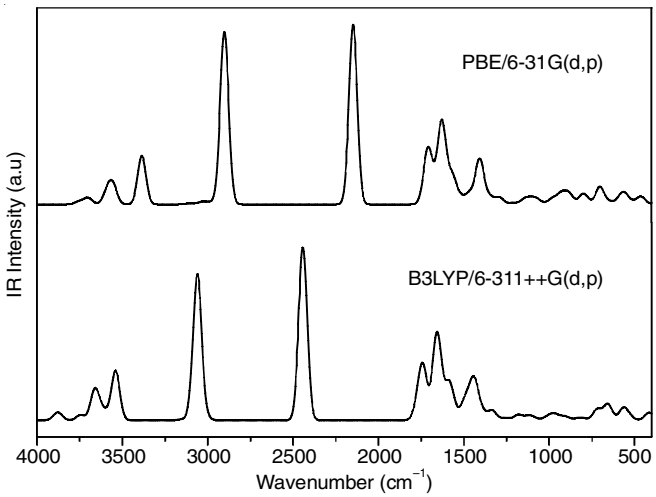

Fig. 10. Theoretically computed FT-IR spectrum of DMTLDH

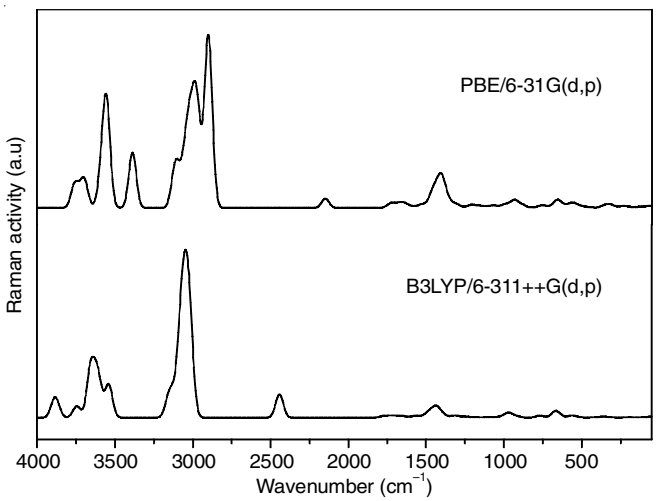

Fig. 11. Theoretically computed FT Raman spectrum of DMTLDH

(NH_2) vibrations occurs at 3619, 3489, 2958, 1648, 1162, 1084, 870 cm^{-1} in B3LYP/6-311++G(d,p) and 3643, 3500, 2957, 1650, 1148, 1085, 865 cm^{-1} in PBEPBE/6-31G(d,p) basis set. Experimentally the medium infrared peak at 1667 cm^{-1} is ascribed to C–N stretching vibration. The observed weak infrared peak at

TABLE-7
WAVENUMBERS (cm^{-1}) AND RELATIVE INTENSITIES OF OBSERVED AND CALCULATED FOURIER INFRARED AND RAMAN SPECTRA OF DMTLDH

B3LYP/6-311++G(d,p)				PBEPBE/6-31G(d,p)				Experimental		Band assignment description
Unscaled frequency	Scaled frequency	IR intensity	Raman activity	Unscaled frequency	Scaled frequency	IR intensity	Raman activity	FT-IR (cm^{-1})	FT Raman (cm^{-1})	
3888	3758	63.55	70.86	3758	3705	35.49	69.57			28O-30H asymmetric stretching
3870	3741	65.82	30.69	3719	3666	36.76	23.74			25O-26H asymmetric stretching
3744	3619	80.05	54.14	3695	3643	66.66	73.81			31N-32H asymmetric stretching/31N-33H asymmetric stretching
3662	3539	356.34	4.86	3590	3540	157.51	64.59			25O-27H asymmetric stretching/4N-5H stretching
3654	3532	118.54	225.02	3562	3512	146.09	143.12			25O-27H asymmetric stretching
3610	3489	137.04	192.48	3549	3500	129.77	190.41			31N-32H stretching/ 31N-33H stretching
3540	3421	749.84	154.09	3386	3339	683.28	167.85	3332s		28O-29H stretching
3155	3050	8.024	66.96	3118	3074	5.69	73.12			11C-14H stretching
3133	3028	10.99	74.73	3099	3056	9.96	73.77			35C-38H stretching/35C-37H stretching
3089	2986	4.504	51.39	3059	3016	3.87	56.16			35C-36H stretching
3087	2983	6.853	36.33	3051	3008	4.03	40.15			18C-19H stretching/18C-20H stretching
3085	2981	71.91	84.02	3028	2986	27.13	108.80			11C-12H stretching/11C-13H stretching
3067	2964	104.84	70.23	3020	2977	4.38	69.99			21C-22H stretching/18C-19H stretching/18C-20H stretching
3061	2958	1987.84	290.54	2999	2957	9.49	133.20		2968w	4N-6H stretching
3051	2948	70.08	111.19	2971	2930	20.91	241.08			18C-19H stretching/18C-20H stretching/21C-22H stretching
3028	2926	7.95	181.66	2968	2926	3.67	24.50	2928	2918w	35C-36H stretching/35C-37H stretching/35C-38H stretching
3026	2925	17.97	232.3	2904	2863	2167.05	373.85	2846		11C-14H stretching/11C-13H stretching/11C-12H stretching
3009	2908	37.85	89.95	2888	2847	299.11	173.39			21C-34H stretching
2443	2361	2623.63	108.95	2147	2117	2518.55	28.18			1N-2H stretching
1774	1715	145.88	6.94	1736	1712	67.70	6.915	1736m		24O-23C stretching
1741	1683	796.99	4.70	1709	1685	724.82	10.61		1697s	4N-3C stretching
1706	1648	24.76	8.41	1673	1650	110.47	4.39	1667m		6H-4N-3C bending/5H-4N-6H bending
1661	1606	901.97	3.59	1659	1636	36.23	7.15	1640w		9N-10C stretching/ 7N-3C stretching
1654	1599	145.21	1.96	1652	1629	31.55	2.52			31N-8C stretching
1646	1591	303.52	0.81	1630	1607	995.35	6.31			31N-8C stretching
1641	1586	21.25	2.51	1613	1591	146.56	3.25		1616s	28O-29H-17O bending
1589	1536	499.44	2.06	1570	1548	379.45	3.24	1530ms		16O-15C stretching/17O-15C stretching
1561	1509	130.28	8.76	1525	1503	100.57	10.18	1523m		7N-8C stretching
1507	1457	36.81	1.65	1482	1461	48.68	3.09			4N-3C stretching
1496	1446	193.65	7.48	1466	1446	62.87	14.90			14H-11C-13H bending/12H-11C-13H bending
1481	1431	49.86	5.93	1456	1436	47.55	11.24			14H-11C-13H bending/12H-11C-13H bending
1480	1430	9.22	5.79	1447	1427	3.34	13.54			37H-35C-36H bending
1466	1417	17.35	7.60	1435	1415	11.60	18.78			37H-35C-36H bending
1459	1410	67.29	1.33	1428	1408	2.82	6.92		1402w	31N-8C stretching/12H-11C-13H bending
1449	1400	86.64	6.67	1411	1391	268.46	9.06			34H-21C-22H bending
1445	1397	184.29	4.76	1406	1387	144.02	3.66			34H-21C-22H bending
1435	1387	176.54	7.57	1402	1382	177.24	57.31			34H-21C-22H bending/34H-21C-22H bending
1430	1382	128.49	28.82	1388	1368	38.47	17.85	1359w	1361m	11C-10C stretching
1396	1349	49	14.17	1368	1349	29.86	15.95			9N-10C stretching/7N-3C stretching
1394	1347	61.97	0.84	1345	1327	78.75	6.72			37H-35C-36H bending
1380	1334	11.28	0.57	1331	1312	6.46	4.15	1311vw		22H-21C-23C bending
1335	1291	138.35	2.96	1309	1291	3.45	4.95		1290	19H-18C-15C-17O Torsion
1311	1267	14.78	8.39	1290	1272	93.73	4.89			7N-8C stretching/7N-3C stretching
1257	1215	31.58	4.82	1213	1196	20.13	8.16	1194w		34H-21C-23C-35C Torsion
1218	1178	1.393	2.45	1172	1156	2.85	5.06			19H-18C-21C bending
1203	1162	10.78	0.06	1164	1148	11.91	0.40			6H-4N-3C bending
1179	1139	75.63	2.72	1139	1123	70.84	3.32	1125	1127w	24O-23C-35C bending
1122	1084	58.81	0.89	1100	1085	68.82	2.35			2H-1N-3C-7N torsion
1099	1062	8.38	1.23	1068	1054	39.35	1.78	1056w		11C-10C stretching

1091	1055	19.43	1.65	1066	1051	13.15	4.26			11C-10C-9N bending/14H-11C-13H-28O torsion/29H-17O-2H-1N torsion
1086	1050	2.42	0.91	1054	1039	2.00	0.51			38H-35C-23C-21C torsion
1062	1027	2.19	0.33	1040	1025	3.73	0.99			11C-1N-9N-10C out
1040	1005	7.35	2.23	1003	988	12.094	5.16			24O-21C-35C-23C out
1009	975	33.58	1.82	981	968	37.87	3.55			7N-8C stretching
997	964	18.78	3.21	977	963	32.99	4.10		964w	21C-18C stretching/35C-23C stretching/18C-17O-16O-15C out
980	948	17.09	2.92	951	938	9.91	0.33			10C-9N-8C bending/11C-10C-9N bending/9N-8C stretching
968	936	58.58	17.39	933	919	107.97	19.58			7N-8C-9N bending
948	916	12.93	1.82	921	908	22.18	2.72			23C-21C stretching/35C-23C stretching/38H-35C-23C-21C torsion
922	891	26.21	5.72	896	884	80.65	3.27	878w		18C-15C stretching/16O-15C-17O stretching
900	870	38.76	1.83	877	865	87.77	7.02	844w		5H-4N-6H-16O torsion
834	806	23.44	0.31	809	797	91.69	0.47	789w		16O-15C-17O stretching
807	780	24.80	0.12	791	780	57.52	0.93		771w	4N-1N-7N-C out/31N-7N-9N-8C out
769	743	6.33	10.12	771	760	19.13	0.61			35C-23C stretching
734	710	3.14	0.02	751	740	4.27	7.49	748vw		4N-1N-7N-3C out/31N-7N-9N-8C out
718	694	162.19	0.95	704	694	128.84	0.51	714m		28O-29H-17O bending
670	647	17.06	26.04	701	691	113.95	2.73	680m		25O-27H-16O bending
660	638	91.42	1.96	655	646	31.34	23.47		659w	25O-27H-16O bending
652	631	131.34	3.09	633	624	12.05	0.71			25O-27H-16O bending
637	616	12.50	4.46	614	605	3.30	3.37	611vw		18C-15C stretching
604	584	0.17	0.14	598	590	5.39	2.37			11C-1N-9N-10C out
590	570	1.70	0.21	582	574	23.98	1.59			32H-31N-8C-7N torsion
572	553	49.90	4.28	577	569	74.48	4.38	550m	567m	10C-9N-8C bending
563	544	68.56	3.12	552	544	90.17	5.48			7N-8C-9N bending
561	542	57.30	1.91	550	542	6.72	2.94			3C-7N-8C bending
547	528	3.253	0.41	542	534	7.05	2.97	529w		4N-3C-7N bending
542	524	9.02	0.61	517	510	7.08	2.42			31N-8C-9N bending
527	509	43.39	2.55	497	490	23.58	2.93	488w		24O-23C-35C bending
467	451	2.11	0.80	461	455	99.12	1.34			24O-21C-35C-23C out
416	402	110.09	1.97	442	436	7.38	1.32			30H-28O-13H bending
371	359	4.87	1.20	368	363	0.77	1.16			35C-23C-21C bending
362	349	21.58	3.33	354	349	21.12	4.30			35C-23C-21C bending
342	331	86.41	1.05	347	342	88.19	1.46		333w	25O-27H-16O-15C torsion
315	304	2.15	1.36	340	335	50.39	1.72			11C-10C-9N bending
298	288	52.07	0.37	320	316	1.74	1.25			18C-15C-16O bending/35C-23C-21C bending
285	276	61.97	0.18	307	303	81.66	7.04			26H-25O-27H-16O torsion
279	269	202.88	0.01	289	285	18.49	0.56			32H-31N-8C-7N torsion/33H-31N-8C-7N torsion
241	233	10.11	0.40	238	234	33.57	3.44			23C-21C-18C bending
222	215	38.69	0.89	236	233	17.95	0.40			17O-2H stretching/17O-29H stretching/16O-27H stretching
205	198	9.80	0.16	230	227	17.41	0.72			11C-1N-9N-10C out
196	189	34.67	0.27	220	217	210.78	0.70			13H-11C-10C-1N torsion
193	187	1.71	0.04	209	206	20.3	0.82			1N-10C-9N-8C torsion/7N-8C-9N-10C torsion/7N-8C-9N-10C Torsion
186	179	45.88	1.40	196	194	8.31	0.36			17O-2H stretching/17O-29H stretching
171	165	4.49	0.16	189	186	3.54	0.11			7N-8C-9N-10C torsion/16O-27H stretching
161	155	2.77	0.41	181	179	1.11	1.18			17O-2H stretching/17O-29H stretching/16O-27H stretching
146	141	19.14	0.21	176	173	2.17	0.43			13H-11C-10C-1N torsion/30H-28O-13H bending
129	125	1.055	0.11	159	157	5.44	0.25			38H-35C-23C-21C torsion
107	104	14.02	0.67	139	137	8.91	0.23			29H-17O-2H bending
99	96	8.70	0.42	131	129	1.00	1.34			15C-17O-2H bending
93	90	6.25	0.65	118	116	0.48	1.21			23C-21C-18C-15C torsion
77	75	0.64	1.49	112	110	3.62	0.73		109vw	2H-1N-3C-7N torsion
71	68.64	2.83	0.56	89	88	6.34	0.32			29H-17O-2H bending
59	57.56	1.69	0.37	81	80	6.37	0.42		79w	23C-21C-18C-15C torsion
52	51.18	6.93	0.68	67	66	2.87	3.23			35C-23C-21C-18C torsion/27H-16O-6H-4N torsion
45	44.24	4.49	0.93	59	58	2.29	0.58			27H-16O-6H bending
30	29.56	1.28	0.98	47	46	1.00	0.82			6H-4N-3C-1N torsion
25	24.70	5.69	1.55	37	36	5.60	1.09			17O-2H-1N bending/27H-16O-6N bending
20	19.83	1.21	0.51	28	27	1.48	0.64			16O-15C-17O-2H Torsion
14	14	0.43	0.53	14	14	1.93	1.29			21C-18C-15C-17O torsion

844 cm^{-1} is attributed to N–H···O torsional vibration. The methylene (CH_3) group attached to one of the carbon atom (C10) in the triazine ring is computed at 3050 and 2925 cm^{-1} in B3LYP and 3074 and 2863 cm^{-1} is PBEPBE method. Experimentally this peak of vibration is observed at 2846 cm^{-1} in the infrared spectrum. The amino group (NH_2) attached to the carbon atom (C3) in the triazine ring is computed at 1683/1685 cm^{-1} in B3LYP/PBEPBE. The corresponding experimental infrared peak is observed at 1697 cm^{-1} with strong intensity. There are many stretching vibrations of C–N bond is computed in the region 1600-930 cm^{-1} in both B3LYP and PBEPBE methods. The weak infrared peak at 1640 and 1402 cm^{-1} and medium infrared peak at 1523 cm^{-1} is attributed to C–N stretching vibration of triazinium ring. The deformation mode of C–N–C triazine ring is theoretically computed at 528 and 524 cm^{-1} in B3LYP and 534 and 510 cm^{-1} in PBEPBE method. Experimentally this deformation mode of C–N–C ring is observed at 529 cm^{-1} with weak intensity in infrared spectrum. The computed peak at 2925/2904 cm^{-1} in B3LYP/PBEPBE is attributed to C–H stretching vibration. The infrared peak at 2846 cm^{-1} in infrared spectrum is due to C–H symmetric stretching vibration. The C–C stretching vibrations are computed theoretically at 1382 and 1062 cm^{-1} whereas the corresponding experimental peak is observed at 1359 and 1056 cm^{-1} in infrared spectrum with weak intensity. The corresponding Raman counterpart is occur at 1361 cm^{-1} with medium intensity.

Vibrational bands of levulinate anions: In, levulinate anion many functional groups *viz.* C–C, C–O, C–H. The C–H vibrations are theoretically computed at 2986, 2948, 2926 and 2908 cm^{-1} in B3LYP and 3016, 2930, 2926 and 2847 cm^{-1} in PBEPBE method. Experimentally observed infrared peak at 2928 and weak Raman peak at 2918 cm^{-1} is attributed to methylene group (CH_3) of levulinate anion. The C–C–H mode of deformation vibration is calculated at 1347/1327 and 1334/1312 cm^{-1} in B3LYP/PBEPBE method, respectively. Experimentally this peak is observed at 1311 cm^{-1} with weak intensity in infrared spectrum. The weak Raman mode of C–C–C–O vibration is observed at 1290 cm^{-1}. Theoretically this peak is computed at 1291/1291 and 1050/1054 cm^{-1} in B3LYP/PBEPBE method. The weak Raman peak at 964 cm^{-1} and weak infrared peak at 878 cm^{-1} is due to C–C stretching vibration. Theoretically, these peaks are computed at 964, 916, 891/963, 908, 884 cm^{-1} in B3LYP/PBEPBE method. The carboxyl mode of vibration (C–O) is observed at 1736 cm^{-1} with medium intensity in infrared spectrum. The C–C–O bending mode of vibration is observed at 1125 and 1127 cm^{-1} in infrared and Raman spectrum, respectively. Theoretically these peaks are computed at 1139 and 1123 cm^{-1} in B3LYP and PBEPBE, respectively. The out-plane bending mode of O–C–C–C vibration is computed at 1005/988 cm^{-1} for B3LYP/PBEPBE method.

Vibrational mode of water molecule and hydrogen bonds: Asymmetric stretching vibrations of water molecule are computed in the region between 3750 and 3400 cm^{-1} in both B3LYP/6-311++G(d,p) and PBEPBE/6-31G(d,p) basis set. Experimentally the broad peak at 3332 cm^{-1} is attributed to O–H asymmetric stretching vibration. Based on crystallographic data, there are 3 types N–H···O hydrogen bond and 4 types of O–H···O hydrogen bond exist in the compound. N–H···O hydrogen bonded system has the bond length of 2.467 Å, 2.804 Å and 2.787 Å and O–H···O hydrogen bonded system has the bond length of 2.813 Å, 2.724 Å, 2.750 Å and 2.875 Å (Table-5). The hydrogen bonded stretching vibrations of N–H and O–H move towards red shift region than free N–H and O–H stretching vibration. The strong band experimentally observed at 1616 cm^{-1} is assigned to deformation of the water molecule. This deformation of the water molecule is computed at 1586/1591 cm^{-1} in B3LYP/PBEPBE methods. O–H···O bending vibrations are computed at 694, 638, 631 in B3LYP and 694, 646, 633 cm^{-1} in PBEPBE method. Experimentally the medium infrared peak at 680 cm^{-1} and weak Raman peak at 659 cm^{-1} is attributed to O–H···O in-plane bending vibration. The out plane bending O–H···O vibrations are computed in the region between 330-100 cm^{-1} in both the methods. The weak Raman peak at 333 cm^{-1} is assigned to O–H···O out-plane bending vibration.

HOMO-LUMO analysis: Characterization of molecular orbital and prediction of reactivity is explained by Frontier molecular orbital analysis. The transition from ground state to first excited energized state is portrayed by one electron excitation from highest occupied molecular orbital (HOMO) to lowest unoccupied molecular orbital (LUMO). The HOMO-LUMO energy is calculated by DFT/B3LYP-6-311++G(d,p) basis set. The HOMO energy is calculated to be -6.892 eV and LUMO energy is calculated to be -1.824 eV. The energy gap between the HOMO-LUMO reflects the chemical activity of the molecule and inculcates the material nature whether it is soft or hard. The calculated energy gap is 5.068 eV, which confirms that the material is less polarizable and less chemical reactivity as well as very stable [30]. Chattaraj *et al.* [31] proposed the concept of philicity, which is very useful in unraveling reactivity of various molecular systems. HOMO-LUMO energies, energy gap, ionization potential ($-\varepsilon_{HOMO}$), electron affinity ($-\varepsilon_{LUMO}$), electronegativity ($\chi = -\frac{\varepsilon_{HOMO} + \varepsilon_{LUMO}}{2}$), global hardness ($\eta = -\frac{\varepsilon_{HOMO} - \varepsilon_{LUMO}}{2}$), chemical potential ($\mu = \frac{\varepsilon_{HOMO} + \varepsilon_{LUMO}}{2}$), global electrophilicity index (ω), global softness ($S = \mu^2/2\eta$) [32-36] and additional electronic charge ($\Delta N_{max} = -\mu/\eta$) of reactants and product have been calculated [37-42]. Fig. 12 gives the HOMO-LUMO plot of DMTLDH. All these parameters are listed in Table-8. Electrophilicity index (ω) is a positive global reactivity index similar to the chemical hardness and chemical potential measures the stabilization in energy by using electronic charge ($\Delta N = -\mu/\eta = 1.719$) from the environment [35]. The direction of the charge transfer is exemplified by the electronic chemical potential of the molecule.

Natural bonding orbital (NBO) analysis: NBO analyses provide the most accurate possible 'natural Lewis structure' picture of ø, as all orbital details are mathematically chosen to include the highest possible percentage of the electron density. A useful aspect of the NBO method is that it gives information about interactions in both filled and virtual orbital spaces that could enhance the analysis of intra- and intermolecular

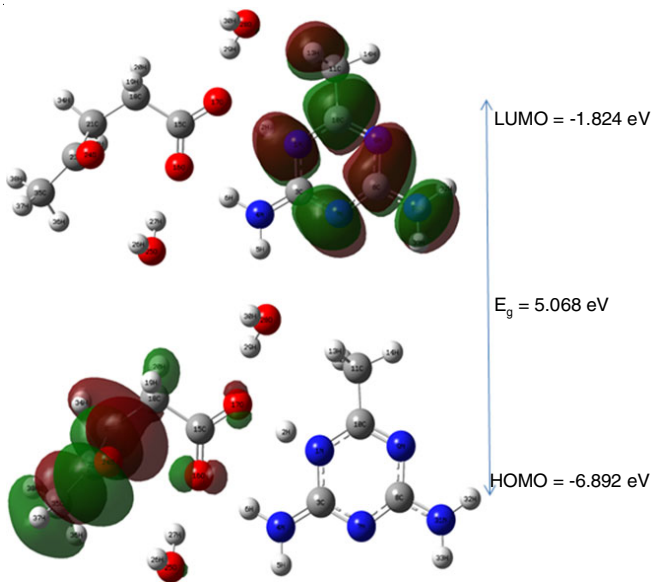

Fig. 12. HOMO-LUMO plot of DMTLDH

TABLE-8
HOMO-LUMO ENERGY VALUE AND RELATED PROPERTIES OF DMTLDH CALCULATED BY B3LYP/6-31++G(d,p) METHOD

E_{HOMO} (eV)	-6.892
E_{LUMO} (eV)	-1.824
Energy gap ΔE (eV)	5.068
Ionization potential (A) eV	+6.892
Electron affinity (I)	+1.824
Global softness (S)	0.197
Global hardness (η)	2.534
Chemical potential (μ)	4.358
Global electrophilicity (ω)	3.747

Interactions. Fig. 13 shows the charges of DMTLDH obtained by NBO analysis. The second-order Fock matrix was calculated to evaluate the donor-acceptor interactions in NBO analysis [43]. The interactions result in a loss of occupancy from the localized NBO of the idealized Lewis structure into an empty non-Lewis orbital. For each donor (i) and acceptor (j), the stabilization energy E2 associated with the delocalization i to j is estimated as:

$$E(2) = \Delta E_{ij} = q_i \frac{(F_{ij})^2}{(E_j - E_i)}$$

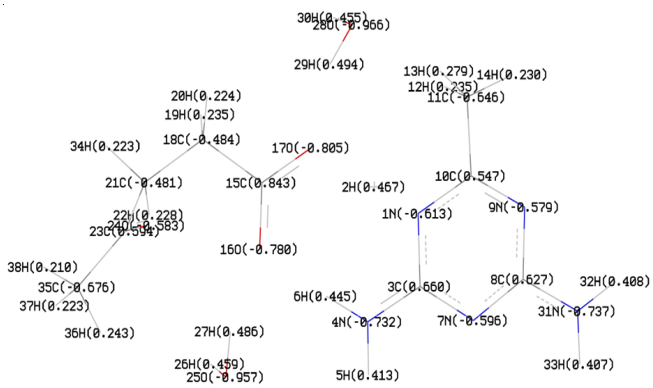

Fig. 13. NBO charges of DMTLDH

where q_i is the donor orbital occupancy, E_i and E_j are the diagonal elements and F_{ij} is the off diagonal NBO Fock matrix element. Within 2,4-diamino-6-methyl-1,3,5-triazinium unit, the highest energy of intra molecular stabilization is found to be 156.12 and 145.40 kJ mol^{-1}, respectively between the donor BD*(2)C3-N4→BD*(2)N7-C8 and BD*(2)N7-C8→BD*(2)-N9-C10. Also the transition between LP(2)O16→BD*(1)N4-H6 20.64 kJ mol^{-1} and LP(2)O17→BD*(1)N1-H2 gives the inter molecular stabilization energy of 43.01 kJ mol^{-1}. Within unit 2 *i.e.* levulinic acid anion the highest stabilization energy is computed to be 92.11 kJ mol^{-1} between lone pair of oxygen atom (O17) and BD*(1)C15-O16. The next highest stabilization energy is computed to be 49.52 kJ mol^{-1} between lone pair of oxygen atom (O17) and BD*(1)C15-O17. The other stabilization energies are listed in Table-9. Being imperative to give the interaction with receptors intermolecular interactions were studied thoroughly. A few ways to deal with quantum chemical modelling of possible interaction of the grown compound with receptors have been used. Establishment of significant intra and intermolecular interactions between the two molecules 2,4-diamino-6-methyl 1,3,5-triazinium with levulinic acid is evidenced by natural bonding orbital analysis.

TABLE-9
SECOND ORDER PERTURBATION THEORETICAL RESULTS OF FOCK MATRIX IN NBO

Donor (i)	Acceptor (j)	$E^{(2)}$ (Kj mol^{-1})	$E_j - E_i$ (a.u)	$F_{i,i}$ (a.u)
Within unit 1				
BD(2)N7-C8	BD*(2)C3-N4	47.87	0.28	0.111
BD(2)N9-C10	BD*(2)N7-C8	34.20	0.31	0.098
LP(1)N1	BD*(2)C3-N4	74.46	0.23	0.118
LP(1)N1	BD*(2)N9-C10	63.41	0.26	0.121
LP(1)N7	BD*(1)N1-C3	11.47	0.79	0.086
LP(1)N7	BD*(1)C8-N9	12.27	0.83	0.091
LP(1)N9	BD*(1)N1-C10	12.29	0.83	0.091
LP(1)N9	BD*(1)N7-C8	11.21	0.88	0.090
LP(1)N31	BD*(2)N7-C8	64.01	0.26	0.119
BD*(2)C3-N4	BD*(2)N7-C8	156.12	0.02	0.072
BD*(2)N7-C8	BD*(2)N9-C10	145.40	0.02	0.071
From unit 1 to unit 2				
BD*(1)N1-H2	BD*(1)C15-O17	3.51	0.13	0.056
From unit 2 to unit 1				
LP(1)O16	BD*(1)N4-H6	6.15	1.09	0.073
LP(2)O16	BD*(1)N4-H6	20.64	0.70	0.109
LP(2)O17	BD*(1)N1-H2	43.01	0.69	0.155
Within unit 2				
BD(1)C35-H36	BD*(2)C23-O24	7.35	0.53	0.056
BD(1)C21-H34	BD*(2)C23-O24	6.87	0.52	0.054
LP(2)O16	BD*(2)C15-O17	15.33	0.77	0.097
LP(2)O16	BD*(1)C15-C18	16.45	0.68	0.096
LP(1)O17	BD*(1)C15-O16	7.61	1.16	0.084
LP(2)O17	BD*(1)C15-C18	12.72	0.73	0.088
LP(3)O17	BD*(1)C15-O16	92.11	0.34	0.160
LP(3)O17	BD*(1)C15-O17	49.52	0.77	0.188
LP(2)O24	BD*(1)C21-C23	20.39	0.66	0.105
LP(2)O24	BD*(1)C23-C35	19.94	0.66	0.104
BD*(2)C15-O16	BD*(1)C15-O16	7.87	0.49	0.123
From unit 2 to unit 3				
LP(1)O16	BD*(1)O25-H27	5.15	1.16	0.069
From unit 2 to unit 4				
LP(1)O17	BD*(1)O28-H29	8.74	1.10	0.088
LP(2)O28	BD*(1)C11-H13	3.09	0.84	0.046

First order hyperpolarizability calculations: The second order electric susceptibility per unit volume establishes the nature of how easily a dipole is induced in a molecule in the presence of an electric field [44]. In present work, 2,4-diamino-6-methyl-1,3,5-triazine with levulinic acid molecular complex has been taken as the subject for first order hyperpolarizability calculation [45-47]. Gaussian 09 program with DFT/B3LYP-6-311G++(d,p) basis set is used to compute the electric dipole moment μ_{tot}, the isotropic polarizability α_{tot} and the first hyperpolarizability γ_{tot}. The calculated values in atomic units (a.u.), are converted into electrostatic units (esu) (α: 1 a.u. = 0.1482 × 10^{-24} esu ; γ: 1 a.u. = 8.6393 × 10^{-33} esu. Table-10 gives the electric dipole moment μ(D), average polarizability α_{tot} (× 10^{-24} esu) and first hyperpolarizability b_{tot} (× 10^{-31} esu). The calculated dipole moment is 4.5478 Debye. The maximum value of dipole moment is found for component μ_x. In this direction, this value is equal to 4.3424 Debye, which means that the molecule is optically reactive in × direction. However, the total polarizability and total first order polarizability is 70.773 × 10^{-24} and 151.517 × 10^{-33} e.s.u, respectively which is slightly more than that of urea (1.31 × 10^{-31} e.s.u). The results of DFT calculations revealed that if suitable dopant is added to the grown crystal will enhance the non-linear optical property and may be considered for nonlinear optical application.

TABLE-10
ELECTRIC DIPOLE MOMENT μ(D). THE AVERAGE POLARIZABILITY α_{tot} (×10^{-24} esu) AND FIRST HYPERPOLARIZABILITY β_{tot} (×10^{-31} esu)

Parameters	B3LYP/ 6-311++G(d,p)	Parameters	B3LYP/ 6-311++G(d,p)
μ_x	4.3424	β_{xxx}	107.6654
μ_y	-0.8987	β_{xxy}	-52.3603
μ_z	-1.0104	β_{xyy}	26.0257
μ(D)	4.5478	β_{yyy}	-26.4117
α_{xx}	-77.9303	β_{zxx}	-17.5487
α_{xy}	-17.3637	β_{xyz}	-7.2812
α_{yy}	-19.1059	β_{zyy}	11.0463
α_{xz}	7.7722	β_{xzz}	1.4758
α_{yz}	-2.7990	β_{yzz}	10.4726
α_{zz}	-115.2824	β_{zzz}	11.2693
α_{tot} (e.s.u)	70.773	β_{tot}(e.s.u)	151.517

Hirshfeld surface analysis: The percentage of intermolecular contacts contributing to the Hirshfeld surface in DMTLDH crystal was resolved by Hirshfeld surface analyses with 2D fingerprint plots. Fig. 14 depicts the fingerprint plot of d_e *versus* d_i which gives the complete information about the involvement of all the intermolecular interactions in the crystal system. Fig. 15 gives the relative contribution interactions of the grown crystal. The study comprises most important interactions of N–H (16.2%), C–H (4.8%), O–H (19.4%) and H–H (51.8%). The bright red spot on carbonyl oxygen and amine nitrogen atom indicates the acceptor and donor of N–H···O interaction of the grown crystal. C–H···O interactions are weak and indicated by weak red spot and H-H interactions are indicated by blue spots. Hirshfeld surface analysis d_i, d_e, d_{norm}, shape index and curvedness of DMTLDH. The planar stacking

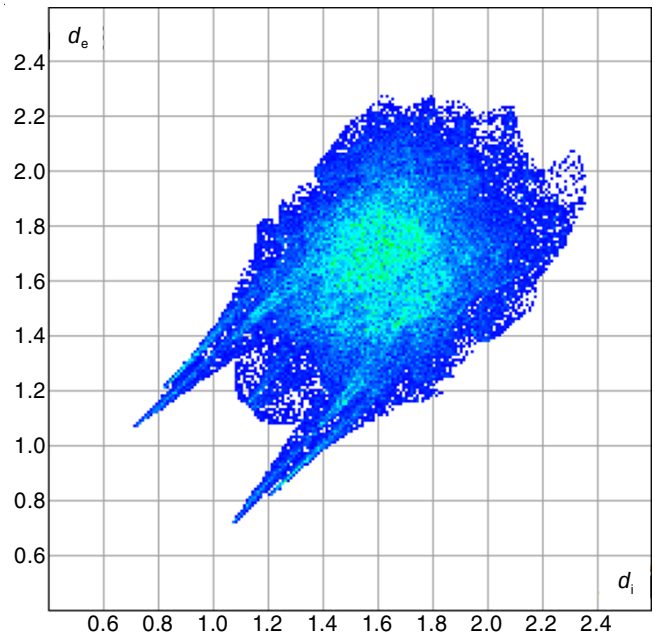

Fig. 14. Fingerprint of DMTLDH (100%)

arrangement and the ways in which adjacent molecules contact with one another is identified by shape index and curvedness plot.

Conclusion

A novel nitrogen rich energetic salt 2,4-diamino-6-methyl-1,3,5-triazinium levulinate dihydrate (DMTLDH) has been synthesized and its structural and vibrational frequencies are analyzed by quantum chemical computational studies using DFT-B3LYP/6-311++G(d,p) and PBEPBE/6-31G(d,p) basis set. The single crystal XRD report of the synthesized salt revealed that the crystal the grown crystal DMTLDH crystallizes in the centrosymmetric space group *P*21/*n* of monoclinic system. The structure is stabilized by C–O···Cg interactions and intermolecular N–H···N, N–H···O, C–H···O, O–H···O hydrogen bonds leads to a formation of a three dimensional network. It is noted that structural as well as vibrational parameters obtained by B3LYP/6-311++G(d,p) yield a comparable results with experimental values than PBEPBE/6-31G(d,p) basis set. The HOMO-LUMO energy gap is calculated to be 5.068 eV and confirms the charge occurrence between the molecules. The hyperconjugative interaction energy and electron densities of donor (i) and acceptor (j) bonds were calculated to study the stability of the molecule by natural bonding orbital analysis. Besides hyperpolarizability calculations have been done and the computed total polarizability and total first order polarizability is 70.773 × 10^{-24} and 151.517 × 10^{-33} e.s.u, respectively indicates that the material may be considered for non-linear optical application. Further, a visually appealing Hirshfeld surface analysis has been carried out to investigate the intermolecular interactions between the molecules in the studied compound. The significant contributions of C–H/N–H/O–H and H-H confirmed the presence of C–H···O, N–H···O and O–H···O intermolecular interactions in the grown compound. Thus, it is believed that all the above mentioned theoretical

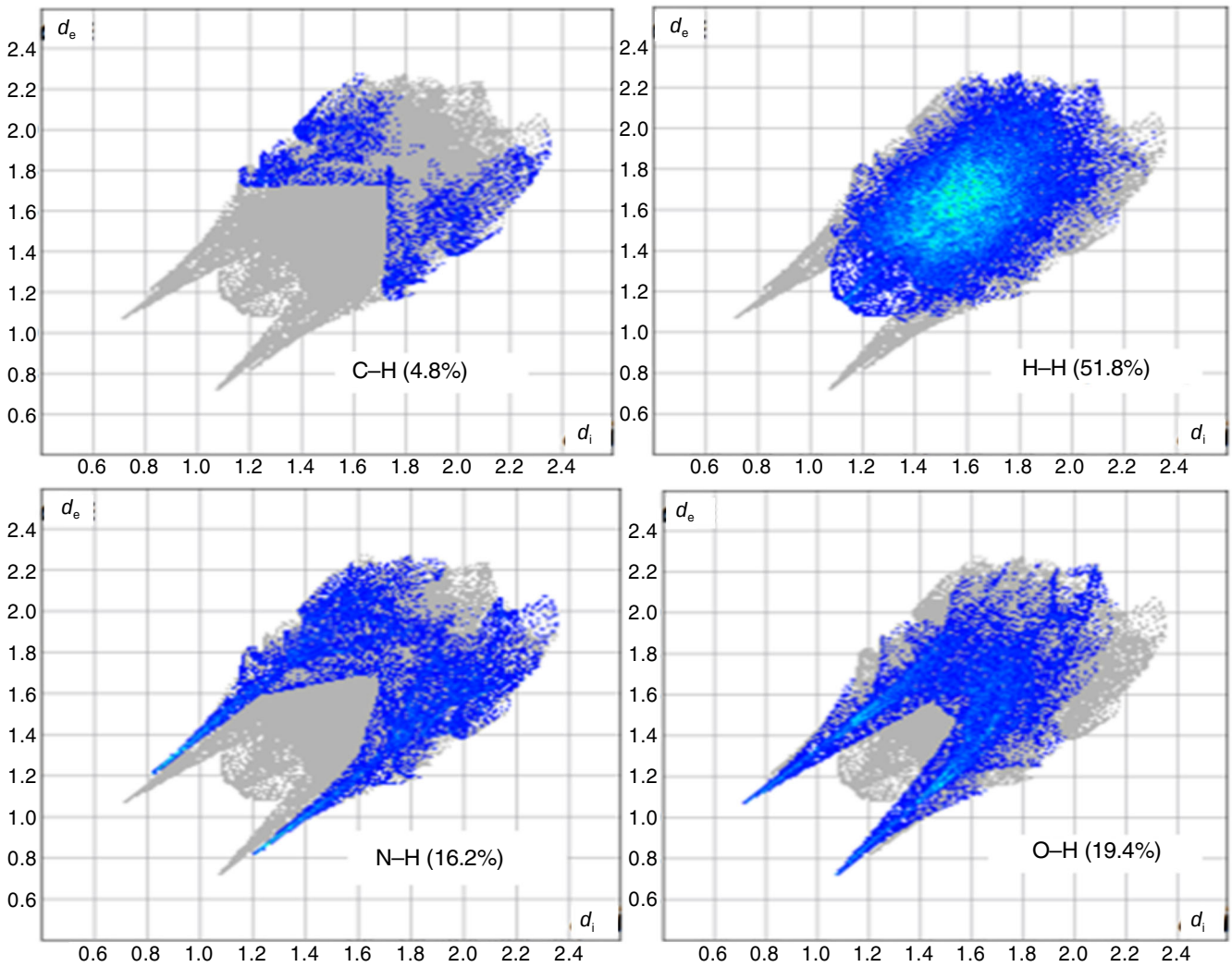

Fig. 15. Two-dimensional fingerprint plots and relative contributions of the atom pairs to the Hirshfeld surface

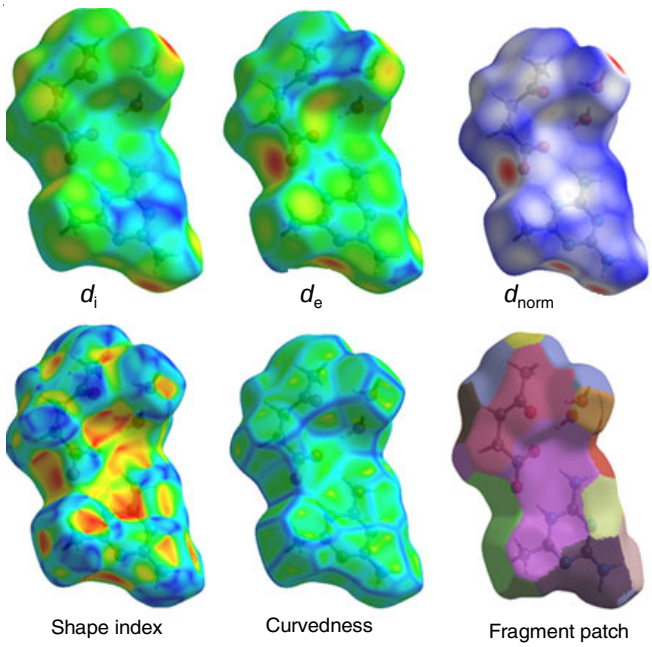

Fig. 16. Hirshfeld surface analysis d_i, d_e, d_{norm}, shape index and curvedness of DMTL DH

structure-property relationship of the grown compound will substantiate the researcher to work on this material for high quality applications.

Supplementary material: Full crystallographic data (cif file) relating to the crystal structure have been deposited with Cambridge Crystallographic Data centre as CCDC 2013604. Copies of this information can be obtained free of charge from the Cambridge Crystallographic Data Centre, 12 Union Road, Cambridge CB2 1Ez. UK (Tel: +44(0) 1223 762911.

CONFLICT OF INTEREST

The authors declare that there is no conflict of interests regarding the publication of this article.

REFERENCES

1. D. Devadiga and T.N. Ahipa, *Liq. Cryst. Rev.*, **7**, 107 (2019); https://doi.org/10.1080/21680396.2019.1666753
2. P. Bhagavath, R. Shetty and D. Sunil, C*rit. Rev. Solid State Mater. Sci.*, **45**, 378 (2020); https://doi.org/10.1080/10408436.2019.1632794
3. K.A. Salmeia, A. Neels, D. Parida, S. Lehner, D. Rentsch and S. Gaan, *Molecules*, **24**, 2672 (2019); https://doi.org/10.3390/molecules24142672

4. E. Benassi, M. Di Foggia and S. Bonora, *Comput. Theor. Chem.*, **1013**, 85 (2013); https://doi.org/10.1016/j.comptc.2013.03.010
5. R. Shanmugakala, P. Tharmaraj, C.D. Sheela and C. Anitha, *Int. J. Inorg. Chem.*, **2012**, 301086 (2012); https://doi.org/10.1155/2012/301086
6. I. Capel Berdiell, R. Kulmaczewski and M.A. Halcrow, *Inorg. Chem.*, **56**, 8817 (2017); https://doi.org/10.1021/acs.inorgchem.7b00699
7. R. Sangeetha, K. Balasubramani, K. Thanigaimani and S. Jose Kavitha, *Acta Crystallogr. Sect. E Struct. Rep. Online*, **74**, 944 (2018); https://doi.org/10.1107/S2056989018008307
8. Z.Y. Xiao, W.Q. Wang, R.Y. Xue, L. Zhao, L. Wang and Y.H. Zhang, *Sci. China Chem.*, **57**, 1731 (2014); https://doi.org/10.1007/s11426-014-5101-3
9. Y. Xiao, B. Jin, R. Peng, J. Zhao, Q. Liu and S. Chu, *J. Mol. Struct.*, **1146**, 417 (2017); https://doi.org/10.1016/j.molstruc.2017.06.030
10. X.-B. Chen, S.-N. Wang, J.-F. Bai and Y.-Z. Li, *J. Coord. Chem.*, **60**, 1941 (2007); https://doi.org/10.1080/00958970601183466
11. Y. Mary, *Int. J. Ind. Chem.*, **2**, 209 (2011).
12. G.J. Perpetuo and J. Janczak, *Acta Crystallogr.*, **C63**, o271 (2007); https://doi.org/10.1107/S0108270107010165
13. L. Narimani and B.M. Yamin, *Acta Crystallogr. Sect. E Struct. Rep. Online*, **68**, o1475 (2012); https://doi.org/10.1107/S1600536812016637
14. K.A. Begam, N. Kanagathara, R. Bhavani, B. Thirumalaiselvam, V. Natarajan, T. Srinivasan and M.K. Marchewka, *Asian J. Chem.*, **32**, 2660 (2020); https://doi.org/10.14233/ajchem.2020.22885
15. V. Ghorpade and M. Hanna, Industrial Applications of Levulinic acid, Cereals, pp. 49-55 (1997).
16. M.J. Frisch, G.W. Trucks, H.B. Schlegel, G.E. Scuseria, M.A. Robb, J.R. Cheeseman, G. Scalmani, V. Barone, B. Mennucci, G.A. Petersson, H. Nakatsuji, M. Caricato, X. Li, H.P. Hratchian, A.F. Izmaylov, J. Bloino, G. Zheng, J.L. Sonnenberg, M. Hada, M. Ehara, K. Toyota, R. Fukuda, J. Hasegawa, M. Ishida, T. Nakajima, Y. Honda, O. Kitao, H. Nakai, T. Vreven, J.A. Montgomery, Jr., J.E. Peralta, F. Ogliaro, M. Bearpark, J.J. Heyd, E. Brothers, K.N. Kudin, V.N. Staroverov, R. Kobayashi, J. Normand, K. Raghavachari, A. Rendell, J.C. Burant, S.S. Iyengar, J. Tomasi, M. Cossi, N. Rega, J.M. Millam, M. Klene, J.E. Knox, J.B. Cross, V. Bakken, C. Adamo, J. Jaramillo, R. Gomperts, R.E. Stratmann, O. Yazyev, A.J. Austin, R. Cammi, C. Pomelli, J.W. Ochterski, R.L. Martin, K. Morokuma, V.G. Zakrzewski, G.A. Voth, P. Salvador, J.J. Dannenberg, S. Dapprich, A.D. Daniels, Ö. Farkas, J.B. Foresman, J.V. Ortiz, J. Cioslowski and D.J. Fox, Gaussian, Inc., Gaussian 09, Revision D.01; Gaussian, Inc.: Wallingford, CT (2010).
17. E.D. Glenening, A.E. Reed, J.E. Carpenter, F. Weinhold, J.A. Bohmann and C.M. Morales, NBO version 5.0, Theoretical Chemistry Institute University of Wisconsin Madison (2001).
18. J.B. Foresman and A. Frisch, Exploring Chemistry with electronic structure methods, Gaussian Inc. Pittsburgh (1996).
19. C.F. Macrae, P.R. Edgington, P. McCabe, E. Pidcock, G.P. Shields, R. Taylor, M. Towler and J. van de Streek, *J. Appl. Cryst.*, **39**, 453 (2006); https://doi.org/10.1107/S002188980600731X
20. M.J. Turner, J.J. McKinnon, S.K. Wolff, D.J. Grimwood, P.R. Spackman, D. Jayatilaka and M.A. Spackman, Crystal Explorer 17 University of Western Australia (2017).
21. S.K. Wolff, D.J. Greenwood, J.J. McKinnon, M.J. Turner, D. Jayatilaka and M.A. Spackman, Crystal Explorer, Version 3.1 (2012).
22. M.A. Spackman, J.J. McKinnon and D. Jayatilaka, *CrystEngComm*, **10**, 377 (2008); https://doi.org/10.1039/B715227B
23. M.A. Spackman and J.J. McKinnon, *CrystEngComm*, **4**, 378 (2002); https://doi.org/10.1039/B203191B
24. M.V. Castillo, R.A. Rudyk, L. Davies and S.A. Brandan, *J. Mol. Struct.*, **1140**, 2 (2017); https://doi.org/10.1016/j.molstruc.2016.08.070
25. K. Diffraction, KM4/CCD Users' Guide, Version 1.169, Wroclaw, Poland (2000).
26. G.M. Sheldrick, X.L.SHEL, Program for Crystal Structure Refinement, University of Gottingen, Germany (1993).
27. G.M. Sheldrick, *Acta Crystallogr. A*, **64**, 112 (2008); https://doi.org/10.1107/S0108767307043930
28. N.B. Colthup, L.H. Daly and S.E. Wiberley, Introduction to Infrared and Raman Spectroscopy, Academic Press: New York (1990).
29. M.P. Fernandez-Liencres, A. Navarro, J.J. Lopez-Gonzalez, M. Fernández-Gómez, J. Tomkinson and G.J. Kearley, *Chem. Phys.*, **266**, 1 (2001); https://doi.org/10.1016/S0301-0104(01)00326-3
30. I. Fleming, Frontier Orbitals and Organic Chemical Reactions, John Wiley & Sons: New York (1976).
31. P.K. Chattaraj, B. Maiti and U. Sarkar, *J. Phys. Chem. A*, **107**, 4973 (2003); https://doi.org/10.1021/jp034707u
32. L.A. Flippin, D.W. Gallagher and K. Jalali-Araghi, *J. Org. Chem.*, **54**, 1430 (1989); https://doi.org/10.1021/jo00267a035
33. R.G. Parr and R.G. Pearson, *J. Am. Chem. Soc.*, **105**, 7512 (1983); https://doi.org/10.1021/ja00364a005
34. P. Geerlings, F. De Proft and W. Langenaeker, *Chem. Rev.*, **103**, 1793 (2003); https://doi.org/10.1021/cr990029p
35. R.G. Parr, L. Szentpaly and S. Liu, *J. Am. Chem. Soc.*, **121**, 1922 (1999); https://doi.org/10.1021/ja983494x
36. P.K. Chattaraj and S. Giri, *J. Phys. Chem. A*, **111**, 11116 (2007); https://doi.org/10.1021/jp0760758
37. M. Nakano, H. Fujita, M. Takahata and K. Yamaguchi, *J. Am. Chem. Soc.*, **124**, 9648 (2002); https://doi.org/10.1021/ja0115969
38. V.M. Geskin, C. Lambert and J.L. Bredas, *J. Am. Chem. Soc.*, **125**, 15651 (2003); https://doi.org/10.1021/ja035862p
39. P.V. Kolinsky, *Opt. Eng.*, **31**, 1676 (1992); https://doi.org/10.1117/12.58844
40. D.F. Eaton, *Science*, **253**, 281 (1991); https://doi.org/10.1126/science.253.5017.281
41. D.A. Kleinman, *Phys. Rev.*, **126**, 1977 (1962); https://doi.org/10.1103/PhysRev.126.1977
42. M. Adant, L. Dupuis and L. Bredas, *Int. J. Quantum Chem.*, **56(S29)**, 497 (1995); https://doi.org/10.1002/qua.560560853
43. P. Manjusha, J.C. prasana, S. Muthu and B. Raajaraman, *J. Mol. Struct.*, **1203**, 127394 (2020); https://doi.org/10.1016/j.molstruc.2019.127394
44. A. Karakas, Y. Ceylan, M. Karakaya, M. Taser, B.B. Terlemez, N. Eren, Y.E. Kouari, M. Lougdali, A.K. Arof and B. Sahraoui, *Open Chem.*, **17**, 151 (2019); https://doi.org/10.1515/chem-2019-0020
45. N. Kanagathara, M.K. Marchewka, G. Anbalagan, A.B. Ahmed and H. Feki, *J. Optoelectron. Adv. Mater.*, **19**, 251 (2017).
46. M. Raja, R.R. Muhamed, S. Muthu and M. Suresh, *J. Mol. Struct.*, **1128**, 481 (2017); https://doi.org/10.1016/j.molstruc.2016.09.017
47. M. Arivazhagan, V.P. Subhasini and A. Austine, *Spectrochim. Acta A, Mol. Biomol. Spectrosc.*, **86**, 205 (2012); https://doi.org/10.1016/j.saa.2011.10.026